Astron. Astrophys. 349, 29–44 (1999)

ASTRONOMY AND ASTROPHYSICS

The temporal characteristics of the TeV γ-emission from Mkn 501 in 1997

II. Results from HEGRA CT1 and CT2

F. Aharonian[1], A.G. Akhperjanian[7], J.A. Barrio[2,3], K. Bernlöhr[1,8], H. Bojahr[6], I. Calle[3], J.L. Contreras[3], J. Cortina[3,2], A. Daum[1], T. Deckers[5], S. Denninghoff[2], V. Fonseca[3], J. Gebauer[2], J.C. Gonzalez[3], G. Heinzelmann[4], M. Hemberger[1], G. Hermann[1], M. Hess[1], A. Heusler[1], W. Hofmann[1], H. Hohl[6], D. Horns[4], A. Ibarra[3], R. Kankanyan[1], M. Kestel[2], O. Kirstein[5], C. Köhler[1], H. Kornmayer[2], D. Kranich[2], H. Krawczynski[1,4], H. Lampeitl[1], A. Lindner[4], E. Lorenz[2], N. Magnussen[6], H. Meyer[6], R. Mirzoyan[2], A. Moralejo[3], L. Padilla[3], M. Panter[1], D. Petry[2,6,9], R. Plaga[2], A. Plyasheshnikov[1], J. Prahl[4], G. Pühlhofer[1], G. Rauterberg[5], C. Renault[1], W. Rhode[6], A. Röhring[4], V. Sahakian[7], M. Samorski[5], D. Schmele[4], F. Schröder[6], W. Stamm[5], B. Wiebel-Sooth[6], C. Wiedner[1], M. Willmer[5], H. Wirth[1], and W. Wittek[2]

[1] Max-Planck-Institut für Kernphysik, Postfach 103980, D-69029 Heidelberg, Germany
[2] Max-Planck-Institut für Physik, Föhringer Ring 6, D-80805 München, Germany
[3] Universidad Complutense, Facultad de Ciencias Físicas, Ciudad Universitaria, E-28040 Madrid, Spain
[4] Universität Hamburg, II. Institut für Experimentalphysik, Luruper Chaussee 149, D-22761 Hamburg, Germany
[5] Universität Kiel, Institut für Kernphysik, Leibnitzstrasse 15, D-24118 Kiel, Germany
[6] Universität Wuppertal, Fachbereich Physik, Gaussstrasse 20, D-42097 Wuppertal, Germany
[7] Yerevan Physics Institute, Alikhanian Br. 2, 375036 Yerevan, Armenia
[8] Now at Forschungszentrum Karlsruhe, P.O. Box 3640, D-76021 Karlsruhe, Germany
[9] Now at Universidad Autónoma de Barcelona, Institut de Física d'Altes Energies, E-08193 Bellaterra, Spain

Received 2 February 1999 / Accepted 28 June 1999

Abstract. We present the results on the TeV gamma emission from Mkn 501 in 1997 obtained with the stand-alone Cherenkov telescopes CT1 and CT2 (threshold ≥ 1.2 and ≥ 1.0 resp.) of the HEGRA collaboration. The CT1 lightcurve has the most complete coverage of all TeV observations of Mkn 501 in 1997 due to the additional observations made under the presence of moonlight. CT2 – at the time of these observations a second generation Cherenkov telescope with relatively low imaging resolution – is a well tested instrument and its 85 hours of observational data on Mkn 501 in 1997 are useful for consistency checks and provide some additional daily data points. The Mkn 501 lightcurve data show significant correlation with the RXTE ASM X-ray data consistent with no time-lag. The spectral analysis shows a steepening spectrum extending beyond 10 TeV. No change of the spectral slope with the variation of the intensity was found. The results presented here are consistent with the results from the HEGRA Cherenkov telescope system presented in part I of this paper.

Key words: gamma rays: observations – galaxies: BL Lacertae objects: individual: Mkn 501

1. Introduction

The BL-Lac object Mkn 501 showed strong and frequent flaring in 1997. The source has been observed by many different experiments using imaging air Cherenkov telescopes (IACTs) (see Quinn et al. 1996, Protheroe et al. 1997, Bradbury et al. 1997 and reference therein).

Here we report on observations with the HEGRA stand-alone telescopes CT1 and CT2 while observations with the HEGRA CT system are reported in part I of this paper (Aharonian et al. 1999, subsequently *Part I*).

From March 11 to October 20, 1997 the source was monitored every night whenever weather and background light permitted it. A fraction of the observations was carried out by up to 6 telescopes.

A detailed discussion of Mkn 501 and its history of γ-emission is given in Part I, as well as the details of the stereo-mode observations with 4 telescopes, the related analysis methods, the stereo-mode results and some comparisons of the stereo-mode data with RXTE observations. The data from the stand alone telescopes CT1 and CT2 are less precise than the system data as energy and angular resolution are somewhat worse. Nevertheless they complement the CT system data as significantly longer observations were carried out. Due to additional observations made under the presence of moonlight the

lightcurve of CT1 is the most complete of all observations in 1997.

This paper has the following structure: Sect. 2 summarizes the relevant telescope parameters of CT1 and CT2 and important performance data. The details of the observations and data analysis are presented in Sect. 3 together with the combined lightcurve. For the comparison with lower energy data from RXTE we include HEGRA observations from 1996. The CT2 data analysis is presented in Sect. 4. The combined lightcurve, specific details and conclusions are discussed in Sects. 5 and 6.

2. The HEGRA Cherenkov telescopes CT1 and CT2

The HEGRA collaboration is operating six imaging atmospheric Cherenkov telescopes for Gamma Astronomy as part of its cosmic ray detector complex at the Observatory Roque de los Muchachos on the Canary island of La Palma (28.75° N, 17.89° W, 2200 m a.s.l., see e.g. Lindner 1997). While the first two telescopes (CT1 and CT2) are operated in stand-alone mode, the other four (CT3, 4, 5 and 6) are run as a system of telescopes in order to achieve stereoscopic observations of the air-showers.

2.1. The telescope CT1

HEGRA CT1 was commissioned in August 1992. In its 1997 configuration, CT1 had a mirror made up of 18 spherical round glass mirrors of 5 m focal length and a total mirror area of 5 m^2. The photomultiplier (PM) camera of CT1 consists of 127 3/4″ EMI tubes 9083A in a hexagonally dense package with an angular diameter of $\approx 3°$ (individual pixel diameter: $0.25°$). The tracking accuracy of CT1 is better than 0.1°. The telescope hardware is described in detail in Mirzoyan et al. (1994) and Rauterberg et al. (1995).

2.1.1. Camera settings and observations under the presence of moonlight

During the 1997 observing period, CT1 was run with a range of slightly different high voltage settings for the PM camera:

During dark nights, two settings were used: Before 29th of April the settings from previous years had been used which we name HV1 in this paper. After the 29th of April, the high voltages were increased by $\approx 6\,\%$ in order to compensate for PM dynode aging effects and to lower the energy threshold of the telescope to below its pre-1996 value. This second setting we denote by HV2.

Soon after the beginning of the 1997 observing period, the strong variability of Mkn 501 made it obvious that it was of great importance to dedicate as much observation time as possible to the source. Until recently, it was believed that Cherenkov telescopes can only operate during moonless nights due to the increase in PM current and noise caused by the general increase in background light. As our studies with CT1 show, this limitation can be largely overcome by fast amplifiers with AC coupling to low-gain PM cameras for which the high voltage is reduced by several percent compared to the optimal setting for moonless nights. The used voltage reduction increases the telescopes threshold by a factor up to 2.6, but observations of strong gamma sources can still give useful results. Details of the observation in the presence of moonlight are given in Kranich et al. (1998).

CT1 has observed Mkn 501 for nearly 7 months whenever the weather fulfilled the standard observing conditions and the source was at zenith angles below $\approx 60°$. The additional observations under the presence of moonlight make the lightcurve obtained from CT1 the most complete one compared to all other 1997 light curves of this source in the TeV energy range. The moonlight observations were taken with four different PM voltage settings: HV1 and HV2 as described above and settings with voltage reduced by 10% and 14% relative to HV2. The latter settings are named HV3 and HV4. Nearly all the data taken under the presence of moonlight were taken with the settings HV1 and HV2. HV4 was used only for observations close to the nearly full moon.

2.2. The telescope CT2

The second HEGRA Cherenkov telescope, CT2, was built in 1993 and has been observing in an essentially unchanged configuration since 1994. CT2 is located at 93 m distance from CT1, i.e. some of the showers are seen simultaneously by both telescopes when operated at the same time. Nevertheless, we treat the observations as independent ones.

CT2 was the prototype for the HEGRA Cherenkov telescope system. As opposed to the equatorially mounted CT1, it has an ALT-AZ mount. The mirror elements are again round glass mirrors of 60 cm ⌀ and 5 m focal length, but 30 instead of 18 are used which give CT2 a mirror area of 8.5 m^2 and thus a lower energy threshold compared to CT1.

In 1997 CT2 was still operated with its original 61 pixel camera with a field of view of 3.7° and an angular diameter of the individual pixel of 0.43°. Studies of the trigger rate as a function of trigger threshold showed that the performance of the telescope has not noticeably changed since 1995 and that the nominal energy threshold of 1 TeV for primary gammas is still valid. The telescope is described in Wiedner (1994) and Petry (1997).

2.3. Performance of the telescopes

Table 1 summarizes some essential parameters of the telescopes. Most of the parameters were determined experimentally while some were calculated from Monte Carlo (MC) simulations. For the MC simulations we used the computational code described in Konopelko et al. (1996). This program includes the losses of Cherenkov light due to atmospheric effects, i.e. Rayleigh and Mie scattering, as well as the telescope parameters such as spectral mirror reflectivity, PM quantum efficiency etc. The simulations took into account the imperfections of the telescope optics and the differences in the CT1 PM noise for the different night sky background (NSB) conditions, e.g. due to the presence of moonlight. The relation between photoelectrons and measured quantities, i.e., the ADC conversion factor, has been determined

Table 1. Main parameters of the HEGRA telescopes CT1 (1997 configuration) and CT2.

	CT1	CT2	comments
mirror area	5 m^2	8.5 m^2	mean reflectivity $\approx 80\%$
camera diameter	3°	3.7°	$\approx 98\%$ active area
pixel no. and size	127; 0.25°	61; 0.43°	
tracking precision	$< 0.1^\circ$	$< 0.1^\circ$	
trigger condition	≥ 2 coinciding pixels each above 12 pe (HV2)	≥ 2 coinciding pixels each above 34 pe	
trigger rate	1.75 Hz (HV2)	2.6 Hz	raw rate in zenith position
trigger rate after filter	1.2 Hz (HV2)	1.4 Hz	rate after filter cuts, in zenith position
threshold in zenith	HV1: 1.8 TeV HV2: 1.2 TeV HV3: 2.4 TeV HV4: 3.2 TeV	1 TeV	
angular resolution	0.13°	0.2°	for single events, mean of axis of error ellipse
collection area	see Fig. 1a-c	see Fig. 1d	
energy resolution	see Fig. 2b	see Fig. 2b	
$Q(\gamma/h)$ after trigger and filter[1)]	13	7.5	refers to entire FOV of camera
$Q(\gamma/h)$[1)]	4.2 (α bin 0–10°)	3.7 (α bin 0–15°)	refers to restricted ALPHA bin
rate for Crab (zenith)	10 over bg. of 6 (HV1)	14 over bg. of 47	
γ/h cuts	dynamic supercuts	static supercuts	
ALPHA cut	$\leq 10^\circ$	$\leq 15^\circ$	for optimal signal/background

1) not including γ enrichment due to trigger

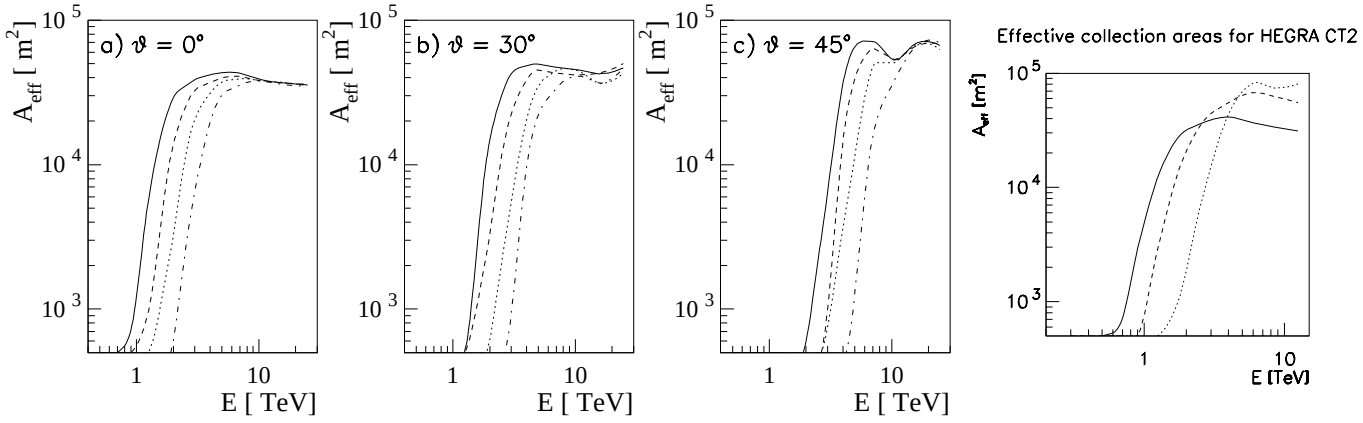

Fig. 1a–c. The effective collection area of CT1 (after gamma/hadron separation cuts) for primary gammas as a function of primary energy for three different zenith angles. The individual lines denote the high voltage settings of the camera: solid line = HV2, dashed line = HV3, dotted line = HV1, dot-dashed line = HV4. The fourth plot shows the effective collection areas of HEGRA CT2 for primary gammas after gamma hadron separation cuts for three different zenith angles: 0° (solid line), 30° (dashed line), 45° (dotted line).

by a separate experiment in 1995/96 for the HV setting HV1, i.e. before the dynode aging. For the other HV settings of CT1 the related change in conversion factors has been calculated from the HV-gain characteristics of the PMs, which were found to be in excellent agreement with the change of trigger rate (after subtracting noise triggers).

The effective collection area depends on the HV setting, zenith angle and used γ/hadron separation cuts. Fig. 1a-c shows the collection area of CT1 for the four HV settings and three different zenith angles and Fig. 1d the areas for CT2, respectively. The image cut procedures are different for CT1 and CT2. For the CT1 data the so-called dynamical supercuts, depending on the zenith angle, the image size and the distance parameters were used, see Petry & Kranich (1997) and Kranich (1997) for details. If the HV setting was the same for moon and non-moon observations, then the difference in NSB only changes the effective collection area at the $< 5\%$ level. This change was taken into account in flux (resp. spectrum) calculations but is too small to be visible in Fig. 1a-c. Standard supercuts were used for CT2 as in Petry et al. (1996) due to the coarse pixel structure of the camera.

The energy reconstruction as well as the energy resolution of both telescopes depend mainly on the image parameter SIZE. The SIZE is in first order a good approximation of the initial

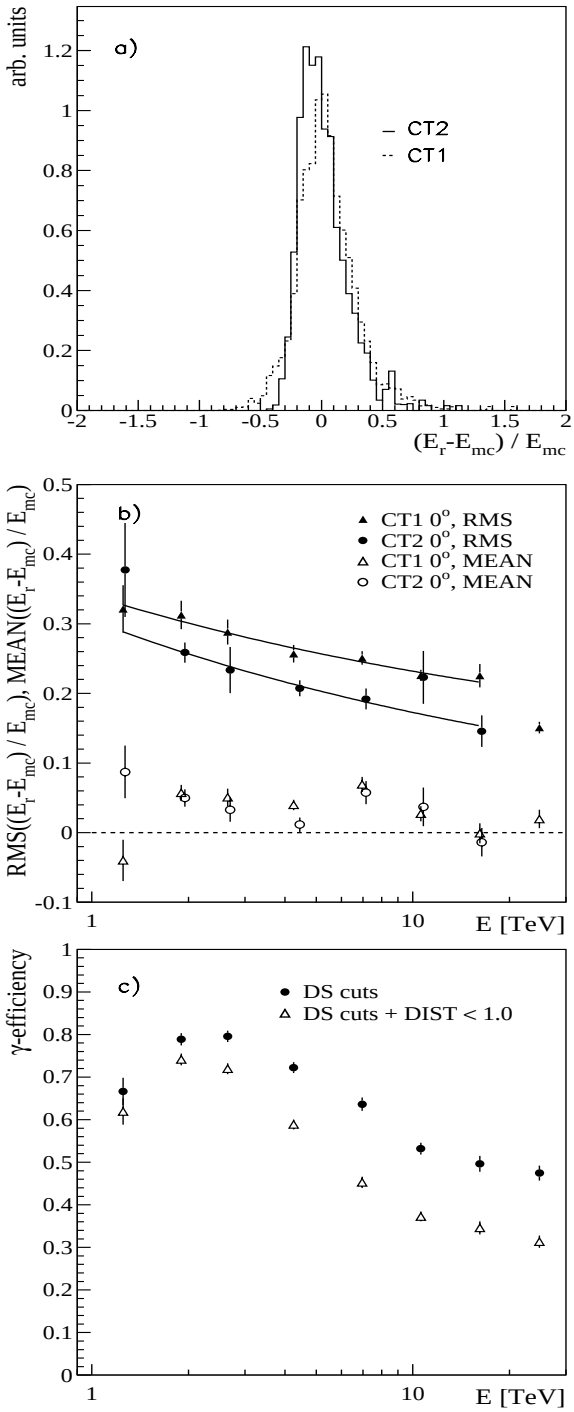

Fig. 2. **a** Comparison between MC input energy and reconstructed energy. For the energy spectrum a power law with a differential coefficient -2.2 is assumed; **b** Predicted energy resolution as a function of γ energy and relative deviation between the mean reconstructed energy and the initial energy. For CT1 and CT2. **c** Overall cut-efficiencies for standard cuts (DS) and for harder cuts used for the spectrum analysis.

γ energy. In second order one has to apply corrections due to the zenith angle and the impact parameter. Also intrinsic fluctuations in the height of the shower maximum, xmax, can affect the energy reconstruction. With a single telescope one cannot determine the impact parameter directly. Nevertheless, the image parameter DIST provides a sufficiently precise measure of the impact parameter, while up to now no equivalent observable for xmax is known. From MC simulations, as well as from accelerator experiments it is known, that electromagnetic showers have a much smaller fluctuation of the depth of the shower maximum compared to hadronic showers. From MC data we developed a correction function which allowed us to calculate the initial energy, as well as predicting the energy resolution from the image parameters SIZE, DIST, WIDTH and the zenith angle. We used the Levenberg-Marquardt method (Marquardt 1963) on MC data to determine the parameters of a Taylor series expansion of the photon energy in the variables SIZE, WIDTH, zenith angle and Exp(DIST^2). Note that the latter term takes empirically into account both, shower image leakage outside the FOV, as well as the drop in light intensity for impact parameters larger than 100 m. For the energy reconstruction studies we used a slightly harder distance cut that does nearly not affect the collection area below 3.5 TeV but reduces the collection area for higher energies by about 25%, see also Fig. 2c. The results obtained by this method on a complementary MC data sample are shown in Figs 2a and 2b.

Fig. 2a shows the distribution of the relative difference between initial and the reconstructed energy for a power law spectrum (differential coefficient: -2.2) above 3.0 TeV. Fig. 2b shows the predicted energy resolution as function of energy. The worse energy resolution of CT1 compared to that of CT2 has its origin, besides the smaller mirror area, in the smaller CT1 camera field of view. At higher energies a considerable amount of Cherenkov light is falling outside the camera and thus information is lost. This loss also affects the angular resolution. It should be noted that the shown RMS values are 10–30% larger compared to standard deviations derived from a gaussian fit. Fig. 2b also shows the relative deviation between mean reconstructed energy and initial energy. The deviation is less than 9% of the initial energy for both telescopes, but has no effect on the derived spectra as the unfolding method (see Sect. 3.1) takes these systematics, both the fluctuation and the small offset in the energy reconstruction, properly into account. A detailed description of this energy reconstruction method will be presented in a forthcoming paper.

3. Observations and data analysis – CT1

Between March and October 1997 we observed Mkn 501 (ON-source data) with CT1 for 380 hours at zenith angles between 11° and 60°. Background data were recorded for a total of 140 h. In order to maximize ON-source observation time, particularly at small zenith angles, the OFF-source data were not taken in ON/OFF cycles but mostly a few hours before or after the Mkn 501 observations. Thus not always the equivalent time for a certain zenith angle setting could be obtained. To compensate for this deficiency we blended the background at a specific zenith angle range from data taken at larger and smaller values. For details (also for the general cutting proceedure) we refer to Petry (1997), Kranich (1997) and Petry & Kranich (1997). It should be noted that the observation time was planned well in advance

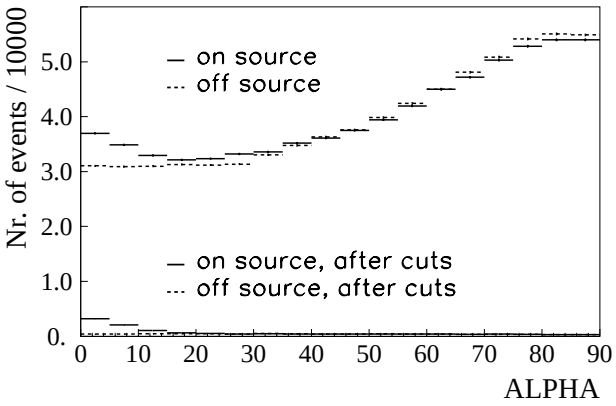

Fig. 3. ALPHA distribution of the raw data after the filter cuts for HV2, zenith angle $< 38^\circ$ (upper data points) and the additional dynamical supercuts (lower data points), see also Fig. 4 for expanded scale.

and that shift operators had no feedback on nightly results such that a bias to prolonged observation in case of large excess was avoided.

The data analysis proceeded in the following order. In a first step of data selection the following criteria were applied:

a) The atmospheric transmission must be high. Whenever available, the atmospheric extinction measurements from the nearby Carlsberg Automatic Meridian Circle (CAMC) were used. For good data, we require the extinction coefficient in the Johnson V-band to be smaller than 0.25.
b) The trigger rate, based on 20 min runs, must be within $\pm 10\%$ of the expected one. This rate is zenith angle dependent.
c) Only data up to 38° zenith angle were used for further analysis. Due to a lack of MC events at large zenith angles the data for $\theta_z > 38^\circ$ will be analyzed later and presented elsewhere.

Since the weather was exceptionally good in 1997 only a few nights were lost due to dense cloud coverage while for the remaining nights always a high atmospheric transmission was given, see Table 4 for the Johnson V values (whenever available). Only 27 hours of data were rejected due to large deviations from the expected trigger rate. Data from 58 hours of observations were deferred for later analysis because the zenith angle exceeded 38°.

Next, so-called filter cuts were applied rejecting mostly noise induced triggers. After the FILTER cut the surviving data present a nearly pure sample of hadronic and γ shower images. For these events the usual Hillas image parameters were calculated. Fig. 3 (upper data points) shows the ALPHA distribution for the ON-source data as well as for the OFF-source data normalized to the ALPHA range between 20° and 80°. Already a clear ON-source excess at small ALPHA values is seen in the raw data.

After the filter cuts, the data are further reduced by applying the above-mentioned dynamical supercuts. These cuts vary with the zenith angle, the image parameter SIZE (a coarse measure of the initial energy) and the image parameter DIST (a coarse measure of the impact parameter). The dynamical cuts enhance significantly the γ/hadron (γ/h) ratio. Hadrons are suppressed by a factor 50–60 while about 60% of the γ showers are retained.

Table 2. Observation times and rates after FILTER for the different HV settings for CT1. Data integrated up to 38° zenith angle; but not separated for moon/no moon samples.

HV settings	HV1	HV2	HV3	HV4
Observation time (h)	104	180	24.5	13.2
Rate after Filter (Hz)	0.61	1.05	0.34	0.18
Excess events	1875	4587	206	42
Significance (σ)	26.2	51.1	8.7	3.9

Fig. 4a shows the ALPHA distribution for the ON/OFF data after the dynamical supercuts (HV2, dark nights only). The data correspond to 153 hours ON-source time. Fig. 4b shows the equivalent moonlight data for one HV setting, HV1 (after April 29th). Table 2 summarizes for the different HV settings the observation times and rates for the ON-source data collected with CT1, as well as the excess signals and significances.

3.1. Average spectrum

In order to derive the energy spectrum from the CT1 data we have used a technique which implicitly takes into account the effects of the finite energy resolution. This technique is well known in high energy physics by the name of "regularised unfolding" and was developed by Blobel (1984). In brief, this procedure avoids the oscillating behavior of the solution to unfolding problems by attenuating insignificant components of the measurements.

The software package "RUN" (Blobel 1996) takes three sets of data: Monte Carlo data, and background data and on-source data after cuts. From this, it produces – using the regularised unfolding technique – the corrected fluxes in bins of the energy with a statistical error estimation. These values are converted into differential flux values by dividing by the energy bin width, or into integral flux values by summing up all contributions above a certain bin number.

Finally, parameters of the spectra are determined by fitting appropriate functions (see below) to the resulting differential or integral spectrum.

In the examination of the spectrum we used only the data from dark night observations[1]. For the energy estimation for each HV setting, a separate Monte Carlo simulation was undertaken and an energy reconstruction function derived (see Sect. 2.3). The energy resolution achieved by this procedure is shown in Fig. 2b. After this reconstruction, the data were combined and subdivided into two separate zenith angle bins according to the zenith angles of the available Monte Carlo Data (0° and 30°). The first bin (0°-21°) corresponded to 73.0 h observation time, the second (21°-38°) to 80.2 h observation time. The lowest energy bin for the combined 0°-21° data set has its

[1] Here we exclude the moonshine-data because of their higher thresholds making the plot less clear.

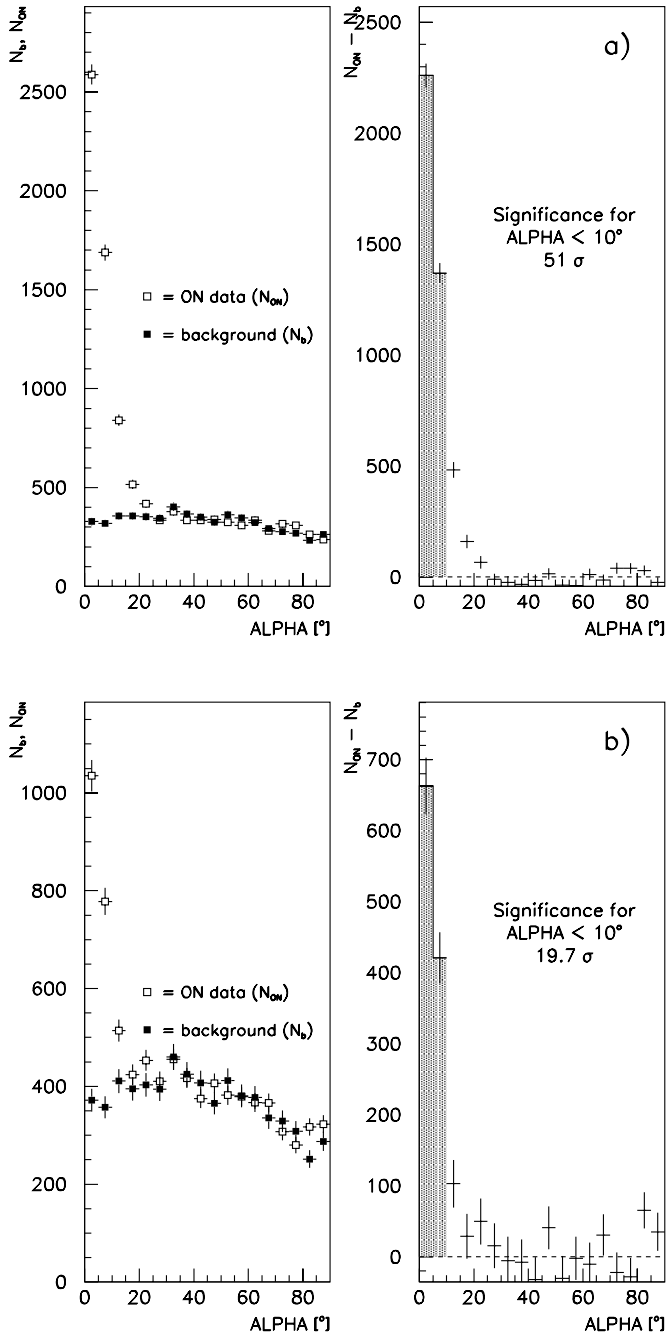

Fig. 4. **a** The total signal from Mkn 501 using all data taken during dark nights with HV2 and up to 38° zenith angle; **b** corresponding distributions with moonshine data for HV1 (moon ≈ 25–60% illuminated).

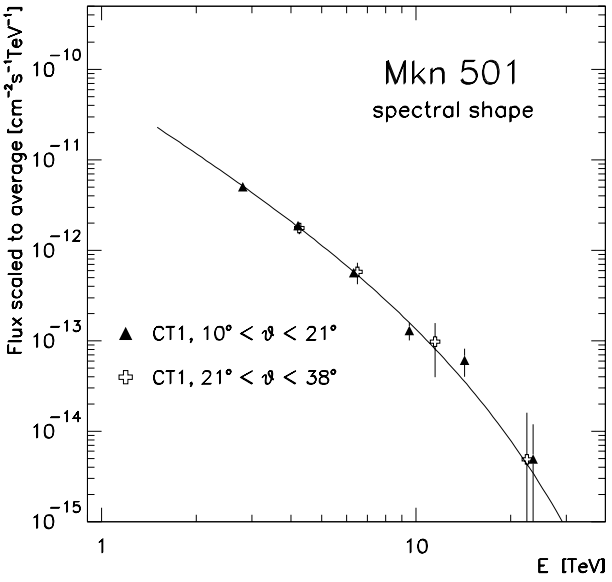

Fig. 5. The average spectral shape as measured by CT1 using the method of regularised unfolding. The solid line represents the result from a power law fit with exponential cutoff. The errors are purely statistical.

threshold at 2.25 TeV, that for 21°-38° at 3.5 TeV[2] The resulting two spectra were scaled such that the fluxes at the point of the lowest common energy were equal. This was done in order to compensate for the time variability of the Mkn 501 emission. The result of the unfolding can be seen in Fig. 5. The comparison with the spectral shape from CT2 and the HEGRA CT system (Part I) is discussed in Sect. 6 (see also Fig. 15).

A power law fit to the 10 data points from CT1 yields a differential spectral index of

$$\alpha = 2.8 \pm 0.07$$

with a reduced χ^2 of 1.1. In the concurrently taken data with the CT system (Part I) and CT2 a significant curvature of the spectrum was seen. These data include measurements at much lower energies and are inconsistent with an unbroken power law. On the other hand the CT1 data are also consistent with the curved spectrum derived from the system and CT2 data, see discussion in Sect. 6.

The unfolding method was tested using data on the Crab Nebula. This data was taken in the years 1995–1997 and amounts to 29 h of observation time. For comparison the results of this are shown in Fig. 6. A power law fit gives a differential spectral index of

$$\alpha_{\mathrm{Crab}} = 2.69 \pm 0.15$$

with a χ^2 of 0.5. This is in good agreement with other measurements of this source (Carter-Lewis et al. 1997, Konopelko et al. 1996, Petry et al. 1996, Tanimori et al. 1998)

3.2. Average flux

For a rapidly varying source, such as Mkn 501 in 1997, an averaged flux is not strictly meaningful because measurements sample the light curve to only 10–20% and the observed variability in time is often similar to the size of the gaps between the daily measurements. Integration over a long period of more than 200 days should nevertheless give a fairly reliable value

[2] The data close to the threshold are affected by large systematic uncertainties and are therefore discarded.

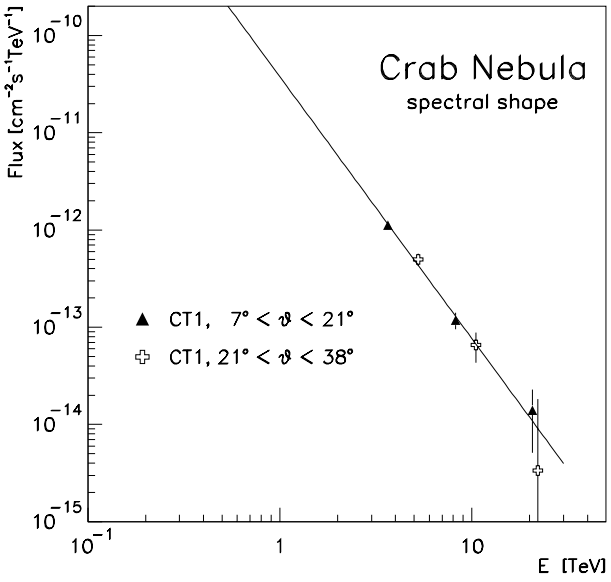

Fig. 6. The spectral shape of the Crab Nebula as measured by CT1 in 1995, 1996 and 1997 (29 h observation time). using the method of regularised unfolding. The superimposed line represents a power law fit. All errors are purely statistical.

on the mean flux. In the following we present the average integral flux above 1.5 TeV. Because of the various HV settings and the threshold variation with zenith angle the threshold was sometimes above 1.5 TeV and extrapolation to 1.5 TeV was necessary. This was performed using a spectral index of 2.8 as determined in Sect. 3.1. The systematic error on the integral flux, arising from the sometimes necessary extrapolation to 1.5 TeV is small. Using a simple power law spectrum with differential index of 2.5 yields only a 5% difference in flux compared to the above spectral parametrisation.

The signal obtained from CT1 observations has a significance of $\approx 58\sigma$ (see Table 2 for the different contributions from the four HV settings). Therefore the statistical error of the average flux is completely negligible. Averaging over the four data sets we obtain the following integral flux above 1.5 TeV

$$F(E > 1.5\ TeV) = 2.33\,(\pm 0.04)_{\rm stat.} \times 10^{-11}{\rm cm}^{-2}{\rm s}^{-1}$$

between March 11th and October 20th. This value can be compared with the Crab Nebula flux above 1.5 TeV. From observations with CT1 in the 1995/96 and 1996/97 winter periods (the same dataset as used for Fig. 6), a Crab flux of

$$F_{\rm Crab}(E > 1.5\,TeV) = 0.82\,(\pm 0.1)_{\rm stat.} \times 10^{-11}{\rm cm}^{-2}{\rm s}^{-1}$$

has been determined (Petry 1997), thus the average flux of Mkn 501 in 1997 was about 3 times larger than that of the Crab Nebula.

The error on the flux is dominated by systematics and reflects only instrument related errors and not those arising from the sparse time sampling. A major contribution to the error comes from the uncertainty for the photon-to-photoelectron conversion which we estimated to be about 15%, which, in turn, converts to a systematic flux uncertainty of $\approx 25\%$. We estimate a total systematic flux error of 30%, common to all flux values.

3.3. Test for time variability of the spectral shape

For the study of Mkn 501's spectral variability above 1.5 TeV we restrict the analysis to the non-moon data taken at HV2 and zenith angles less than 38° because the thresholds of the individual data sets were below 1.5 TeV. For observations lasting longer than 0.5 hours we calculate daily values of $F_{1.5-3}$, the flux between 1.5 and 3 TeV and F_3, the flux above 3.0 TeV. The hardness ratio

$$r_h = \frac{F_3}{F_{1.5-3}}$$

which is available for over 100 nights, can then be inspected for variability.

Fig. 7 shows the result of this study. Only points with significance $> 1\sigma$ were used for the calculation of r_h while the points with $\leq 1\sigma$ were converted to 90% confidence level upper limits and are only shown in the light curves.

There is no indication of significant spectral variability with time, nor of a correlation between the hardness ratio and the emission state. The averaged hardness ratio of 0.41 ± 0.02 (error purely statistical) is somewhat smaller than the ratio of 0.51 ± 0.01 as expected from the spectrum measured by the CT system and CT2 (Sect. 4), but the difference is in the range of the systematic errors.

In order to estimate the degree of variability still permitted by this measurement, we fit a linear function to the plot r_h versus $F_{1.5-3}$ and obtain

$$\begin{aligned} r_h \;=\; & (0.006 \pm 0.007) \cdot F_{1.5-3}[10^{-11}{\rm cm}^{-2}{\rm s}^{-1}] \\ & +(0.39 \pm 0.028) \end{aligned}$$

with a reduced χ^2 of 0.98. With the range of values of $F_{1.5-3}$ of roughly $(0.5\,{\rm to}\,10) \times 10^{-11}{\rm cm}^{-2}{\rm s}^{-1}$, this means that r_h may vary by up to 15% of its average value within the 1σ error of the fit.

We tested the ratio also for a longterm steady change by fitting the expression

$$r_h(t) = c + \alpha \cdot t,\ t\ {\rm in\ days}\ [569 - 714]$$

to the data of Fig. 7c. The fit yielded $\alpha = -0.00093\,, c = 0.98$ and a reduced $\chi^2 = 0.9$. There is no compelling evidence for a longterm change in r_h.

3.4. The CT1 lightcurve above 1.5 TeV

The lightcurve from CT1 data which we present in this paper aims for a time coverage as complete as possible and at the same time minimizing systematic errors from varying zenith angle distributions. In order to achieve this compromise we limit the data set to zenith angles of below 38°. The complete lightcurve of the integral fluxes above 1.5 TeV is shown in Fig. 14 together with the results from the other HEGRA telescopes.

The lightcurve as shown in Fig. 14 is calculated for a threshold of 1.5 TeV. The data are taken from the different HV settings using the above mentioned extrapolation procedure. Only statistical errors are shown.

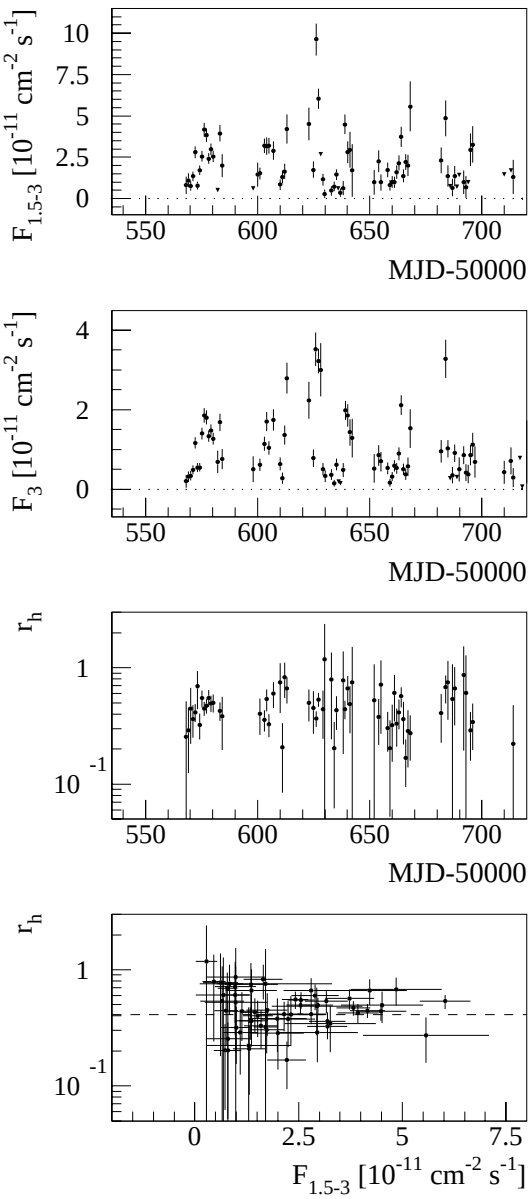

Fig. 7. **a** The photon flux $F_{1.5-3}$ of Mkn 501 at energies between 1.5 and 3.0 TeV from the CT1 data taken with HV2. **b** The photon flux at energies above 3.0 TeV obtained from the CT1 data taken with HV2. **c** The hardness ratio r_h as defined in the text plotted versus time. **d** The hardness ratio plotted versus the flux between 1.5 and 3.0 TeV. The fit of a constant function gives $r_h = 0.41 \pm 0.02$ and a reduced χ^2 of 0.97.

The small possible error of $\mathrm{r_h}$ up to 15%, see previous section, could only influence those points where one has to extrapolate over a sizable energy range, i.e. for the few data points taken at HV4. A listing of the CT1 and CT2 observation times and fluxes is given in Table 4 together with the Johnson V extinction coefficients (whenever available). Note that the MC simulation takes a mean loss of light of 16% into account.

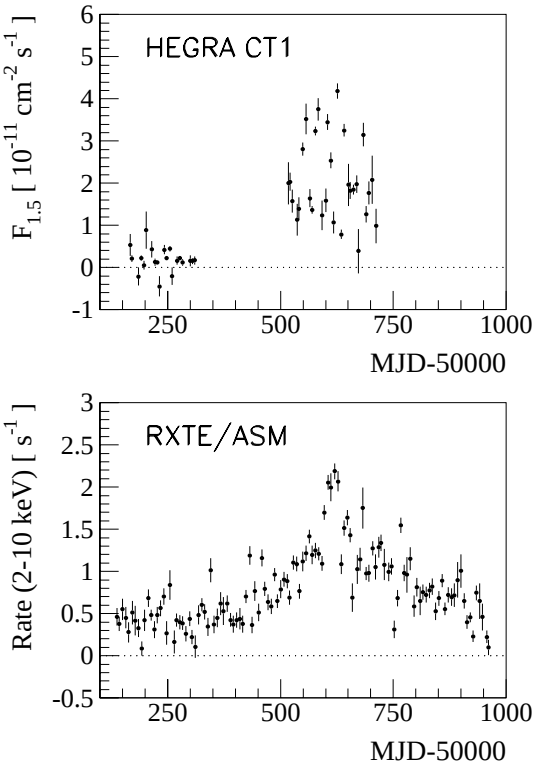

Fig. 8. Observations of Mkn 501 in 1996 and 1997 at energies above 1.5 TeV (using HEGRA CT1) compared to the X-ray emission between 2 and 10 keV as measured by RXTE ASM. In both plots, each point represents the emission averaged over a period of 7 days.

3.5. Correlation with RXTE observations of Mkn 501

Since the beginning of 1996, the RXTE all sky monitor (ASM) has been observing Mkn 501 in the 2–12 keV band.

In Fig. 8, we present the RXTE keV rate together with the data from HEGRA CT1 which observed Mkn 501 both in 1996 and 1997. The simultaneous change in flux in both energy ranges is clearly visible.

In order to further examine the correlation, we plot the daily RXTE averages versus the flux values from the complete CT1 lightcurve in 1997. This is shown in Fig. 9. We obtain a correlation coefficient (see Part I for details) of:

$$r = 0.611 \pm 0.057.$$

with a significance of $8.56\,\sigma$ (based on the assumption of 125 independent data pairs).

In order to verify whether this correlation is real or only an artifact of some binning effects (e.g. fewer observations during moonshine nights, etc.) or unequal data statistics, we shift the CT1 and the RXTE light curves with respect to each other in steps of 1 day by up to ± 100 days. For each shift, we recalculate the correlation coefficient. The result is plotted in Fig. 10. The fact that only at the un-shifted value there is a clear peak visible, underlines the significant correlation between the TeV and keV datasets. Even if we assume that the daily TeV data are highly correlated, i.e., only $1\,/\,5$ of the data is independent, we obtain still a significance of $3.7\,\sigma$.

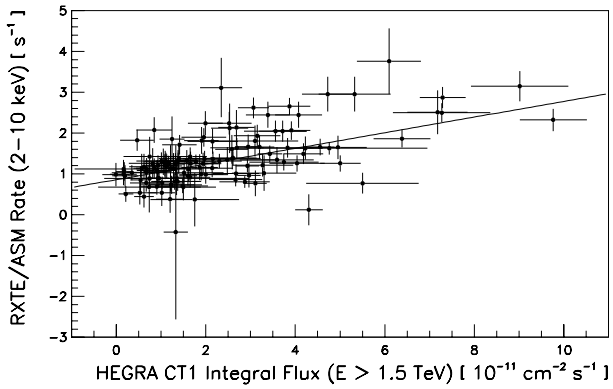

Fig. 9. Correlation between the X-ray emission of Mkn 501 in 1997 as measured by RXTE and the emission above 1.5 TeV as measured by CT1. A linear fit to the data points yields: RXTE Rate $= (0.20 \pm 0.01) \times \mathrm{CT1} + (0.86 \pm 0.04)$ Hz, where CT1 represents the flux above 1.5 TeV in units of 10^{-11} cm^{-2} s^{-1}.

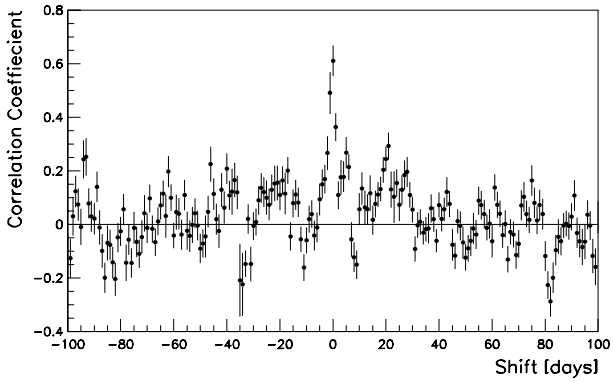

Fig. 10. Check of the correlation between the X-ray emission of Mkn 501 in 1997 as measured by RXTE and the emission above 1.5 TeV as measured by CT1. Plotted is the correlation coefficient as a function of the artificially introduced shift between the RXTE and the CT1 time.

Due to the nearly continuous CT1 observation only a modest modulation due to the lunar period is visible.

The ratio

$$R_{\mathrm{TeV/keV}} = \frac{\langle F_{1.5} \rangle}{\langle \mathrm{RXTE\ countrate} \rangle}$$

(here in units of [10^{-11} cm^{-2} s^{-1}/Hz]) is quite different in 1996 and 1997:

$$R_{\mathrm{TeV/keV}}(\mathrm{MJD\ 50160–50310}) = 0.5 \pm 0.04$$

and

$$R_{\mathrm{TeV/keV}}(\mathrm{MJD\ 50520–50720}) = 1.75 \pm 0.04.$$

While the keV flux rises by about a factor 3 from the 1996 to 1997 periods, the TeV γ flux increases by 11, i.e., about in quadrature of the keV flux.

4. Observations and data analysis – CT2

CT2 observed Mkn 501 between 16 March and 28 August 1997. After thorough checks of the data quality, 85 hours (79 *h* in normal- and 6 *h* in reverse tracking mode[3] rotation of the telescope) of good data remained.

Table 3. The CT2 data sets taken in normal-tracking mode (as used in Fig. 11, 12 and 13) for 3 zenith angle ranges. a) The large reduction by the filter cuts has its origin in fake triggers from muons passing the Plexiglas focons of the PM camera and in the exclusion of the outer pixel ring from the software trigger. b) The quoted significance is slightly different from a value calculated directly from the given excess and background rate. The difference has its origin in a somewhat different background density population as a function of zenith angle.

zenith angle range	$0^\circ - 21^\circ$	$21^\circ - 38^\circ$	$38^\circ - 51^\circ$	total
Observation time (h)	48.3	24.7	6.0	79
Av. Rate before filter (Hz)	2.57	2.62	2.54	
Av. Rate after filter (Hz)[a)]	1.40	1.35	0.85	
background (ALPHA $< 15^\circ$)	1211	862.2	332.5	
excess signal (ALPHA $< 15^\circ$)	2181	1147	196.5	
significance[b)]	25.7σ	$21.06\ \sigma$	6.6σ	34

For the background determination the same procedure was followed as for CT1. The OFF-source data set consisted of 90 hours of data which had passed the same quality cuts as the ON-data and spanned all zenith angles up to 51°.

For the gamma/hadron separation, we employed the set of image parameter cuts already used in Petry et al. (1996). The efficiencies of these cuts and the corresponding Monte Carlo studies are described in Bradbury et al. (1997) and Petry (1997). The effective collection areas of CT2 after gamma/hadron separation cuts for three different zenith angles are shown in Fig. 1d. The characteristics of CT2 have not changed over a long time. This was checked by comparing data from Mkn 421 observations taken in 1995 with the 1997 Mkn 501 data set. Neither the background rates nor the background image parameter distributions of CT2 have changed significantly.

Table 3 summarizes the observation times and trigger rates before and after the FILTER cut for CT2 for 3 ranges of the zenith angle. Also given are the excess and background rates and signal significances after the "image" cuts. Due to the coarser camera pixel size, an ALPHA cut at 15° is applied.

Fig. 11 shows the CT2 ALPHA distributions after all cuts, for the zenith angle ranges as listed in Table 3. In all distributions a clear excess at small ALPHA is seen.

4.1. Average spectrum and flux

For the study of the spectrum of the CT2 signal we applied the regularised unfolding method as for CT1 (see Sect. 3.1). We subdivided the dataset into three separate zenith angle bins according to the zenith angles of the available Monte Carlo data (0°, 30° and 45°) (see Table 3 for statistics).

[3] Normal- and reverse mode refer to the Azimuth range the Telescope is operated when observing a source. The Azimuth range of the reverse mode refers to a 180° rotation in φ

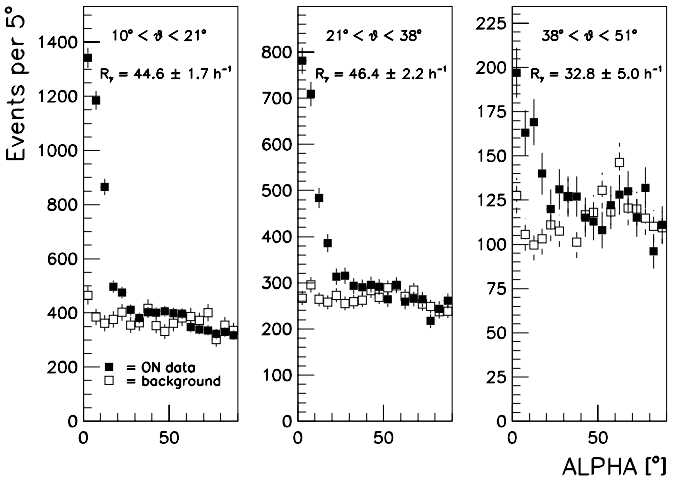

Fig. 11. The ALPHA distributions after all cuts for all normal-tracking data from Mkn 501 observations with CT2 in 1997, split up in three zenith angle (ϑ) bins. R_γ denotes time averaged rates.

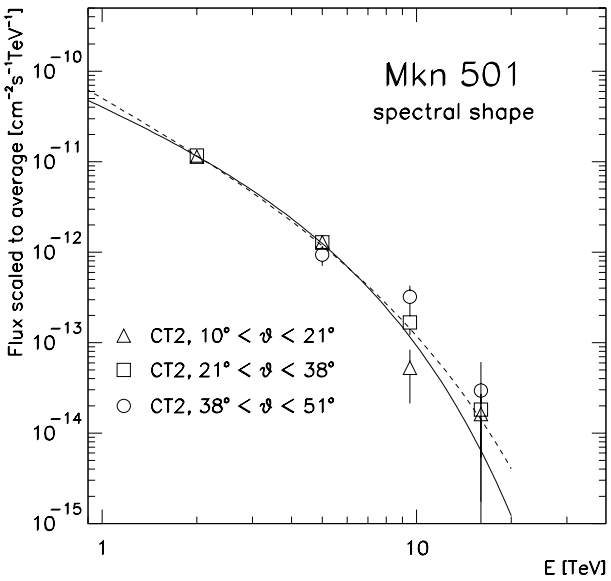

Fig. 12. The average spectral shape as measured by CT2 using the method of regularised unfolding. The curves represent the results from the following fits: Solid line: fit of a power law with exponential cutoff, Dashed line: fit of a power law with fixed index 1.9; exponential cutoff is at 5.3 TeV (see Sect. 6).

For each of these datasets the regularised unfolding was applied separately. The resulting three spectra were scaled such that the fluxes at the point of the lowest common energy were equal. This was done in order to compensate for the flux variation with time. The results are shown in Fig. 12.Within the errors, the spectra from different zenith angle observations are perfectly compatible.

When fitting the CT2 data by a pure power law, we obtain a differential spectral index of

$$\alpha = 2.7 \pm 0.2$$

with a reduced χ^2 of 5.0. In order to improve the fit, we introduce an exponential cutoff, i.e. we fit

$$\mathrm{d}F/\mathrm{d}E \propto E^{-\alpha} \cdot e^{-E/E_0}.$$

This fit gives $\alpha = 1.27 \pm 0.37, E_0 = (2.85 \pm 0.58)\mathrm{TeV}$ with a reduced χ^2 of 1.7. This is shown in Fig. 12 as a solid line.

Using the CT2 data and the above spectrum (when an extrapolation was necessary), we calculate an average flux above 1 TeV

$$F(E > 1.0\ \mathrm{TeV}) = 5.26\,(\pm 0.13)_{\mathrm{stat.}} \times 10^{-11}\mathrm{cm}^{-2}\mathrm{sec}^{-1}$$

for the 85 hours of observation time.

The corresponding Crab flux value measured with CT2 is (Petry et al. 1996):

$$F^{\mathrm{Crab}}(E > 1.0\ \mathrm{TeV}) = 1.57\,(\pm 0.24)_{\mathrm{stat.}}(+0.99\text{–}0.39)_{\mathrm{syst.}} \times 10^{-11}\mathrm{cm}^{-2}\mathrm{sec}^{-1}\,.$$

Here we use the Crab flux as determined by CT2 and not with CT1 because the ratio $F^{\mathrm{Mkn\ 501}}/F^{\mathrm{Crab}}$, when measured with the same telescope, should be free of some systematic errors, such as the photon to ADC signal conversion error. The resulting flux ratio $F^{\mathrm{Mkn\ 501}}/F^{\mathrm{Crab}}$ is 3.3 ± 0.5 and in good agreement with the ratio obtained from the CT1 data (Sect. 3.2).

4.2. Test for time variability of the spectral shape

As for CT1 (Sect. 3.3), we examine the possible spectral variability of Mkn 501 in the independent CT2 data set. Again, we construct from Monte Carlo data a function which estimates the energy of the primary photon from the zenith angle and the image parameters SIZE, DIST and WIDTH (see also Fig. 2b).

For the daily measurements lasting longer than 0.5 hours, we determine the flux F_{1-3} between 1.0 and 3.0 TeV and the flux F_3 above 3.0 TeV and define a hardness ratio r_h as

$$r_h = \frac{F_3}{F_{1-3}}.$$

Note that this is different from the hardness ratio defined for CT1 since the threshold of CT2 is lower. Only data up to a zenith angle of 30° were used.

In Fig. 13 we plot F_{1-3}, F_3 and r_h versus time and in addition r_h versus F_{1-3} to test a dependence on the emission state of the source. A fit of a constant function to the latter plot results in

$$r_h = 0.18 \pm 0.012$$

(errors purely statistical) which is in agreement with the value 0.24 ± 0.02 expected from the measured spectrum if we take into account the large systematic errors of the energy calibration of $\approx$ 20%. given the good reduced χ^2 of 0.92, there is no indication for a correlation between the hardness ratio and the emission state.

As for the corresponding CT1 data, we give an estimate of the degree of variability still permitted by fitting a linear function to the plot r_h versus F_{1-3}. We obtain

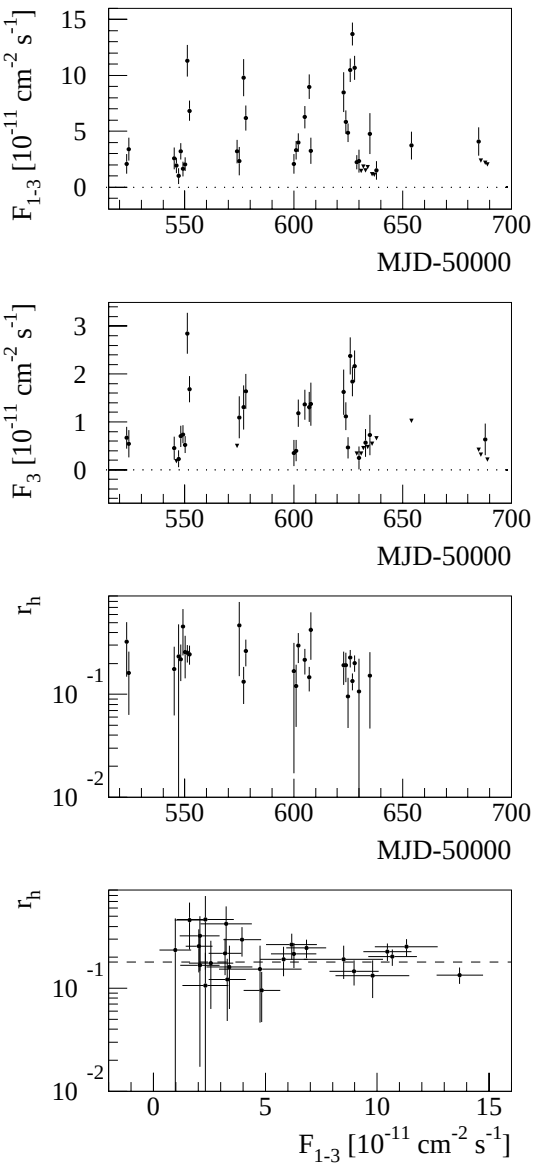

Fig. 13. **a** The photon flux of Mkn 501 at energies between 1.0 and 3.0 TeV determined from the CT2 data. **b** The photon flux at energies above 3.0 TeV obtained from the CT2 data. **c** The hardness ratio r_h, as defined in the text, plotted versus time. **d** The hardness ratio plotted versus the flux between 1.0 and 3.0 TeV. The fit of a constant function gives $r_h = 0.18 \pm 0.012$ and a reduced χ^2 of 0.92.

$$r_h \;=\; (-0.0038 \pm 0.0032) \cdot F_{1-3}[10^{-11}\mathrm{cm}^{-2}\mathrm{s}^{-1}] \\ +0.215 \pm 0.032.$$

(Note again that r_h is differently defined for CT1 and CT2). With the range of values of F_{1-3} of roughly $(1-14) \times 10^{-11}\mathrm{cm}^{-2}\mathrm{s}^{-1}$, this means that r_h may vary by up to 25% of its average value within the 1σ error bars of the fit. However, the fact that the slope in the corresponding result of CT1 has the opposite sign, is an indication that indeed no spectral variability is present.

4.3. The CT2 lightcurve above 1.5 TeV

In order to examine the time variability of the emission of Mkn 501 and to compare the data with those of the other telescopes, we construct the lightcurve above 1.5 TeV. We exclude again the data with zenith angles larger than 38° in order to avoid possible systematic errors due to low MC statistics at large zenith angles.

Each point is calculated according to the method of the adjustment of the zenith angle distribution (see Sect. 3). The errors are purely statistical. The results are shown in Fig. 14 as open circles.

CT2 observations were partly overlapping in time with CT1 or the CT system and partly carried out alone. Therefore the CT2 measurements provide cross checks of the CT1 and CT system measurements and they add some new data points to the lightcurve. The daily fluxes and observation times are listed in Table 5, again for zenith angles below 38° and $E > 1.5$ TeV.

5. The combined CT1, CT2 and CT system lightcurve above 1.5 TeV

In Fig. 14 the lightcurve from all HEGRA CTs is shown for an energy threshold of 1.5 TeV. The observations with CT1 under the presence of moonlight are indicated separately. The errors are purely statistical.

In general we see good agreement between the data from the three instruments. Restricting the comparison to directly overlapping days we obtain the following ratio between the fluxes

$$\frac{F(\mathrm{CT1})}{F(\mathrm{CTsystem})} = 0.73 \pm 0.02, \quad \frac{F(\mathrm{CT2})}{F(\mathrm{CT1})} = 1.03 \pm 0.04$$

and

$$\frac{F(\mathrm{CT2})}{F(\mathrm{CTsystem})} = 0.89 \pm 0.03.$$

The overlap times were 110 h, 60 h and 65 h, respectively. The seemingly small inconsistency in the ratios has its origin in different overlap times and different zenith angles. The ratios agree well within the systematic errors, which are in the order of 30%. The systematic error is in part global and in part quite different for each instrument. There are 5 data points where the disagreement between simultaneous observations with different telescopes differ by more than 4 σ (MJD 50579, 50580, 50582, 50607, 50658) after normalizing the fluxes to the respective mean fluxes. These large differences are for the time being unexplainable. Part of the difference might be due to source variability and different observation times in compared nights but some of the discrepancies remain even for exactly matching ON time slices.

Here we would like to comment on various features of the lightcurve.

1. The largest flare was observed at MJD 50626-27 with a flux above 1.5 TeV of $\approx 10^{-10}$ cm^{-2} sec^{-1}.
2. Other experiments, Whipple and CAT, have observed a large and short flare on April 16th (MJD 50554). Due to complete cloud coverage, HEGRA could not observe that.

Table 4. Diurnal flux values above 1.5 TeV as measured by CT1. For nights with moon- and non-moon observations these fluxes are calculated as the weighted mean. The Johnson V extinction coefficients (from the Carlsberg Automatic Meridian Circle) are stated when available.

Start [MJD]	Φ (E > 1.5 TeV) [10^{-11}cm^{-2}s^{-1}]	Duration [h]	Extinction [JohnsonV]
50517.16	2.00 ± 0.50	1.82	
50518.17	1.49 ± 0.57	1.35	
50519.16	1.50 ± 1.13	0.45	
50520.16	2.87 ± 0.57	1.87	
50521.15	2.67 ± 0.52	2.11	
50522.15	1.21 ± 0.41	2.08	
50523.15	1.86 ± 0.41	2.47	
50525.17	1.65 ± 0.46	1.65	
50526.16	1.66 ± 0.41	2.61	
50527.21	1.31 ± 0.53	0.92	
50528.20	0.94 ± 0.53	1.15	
50536.11	1.00 ± 0.56	2.45	0.15
50537.11	1.24 ± 0.51	2.97	0.14
50539.12	2.16 ± 0.53	2.82	
50540.13	0.98 ± 0.34	2.87	0.13
50545.18	0.53 ± 0.37	1.24	
50546.09	1.20 ± 0.31	3.41	0.10
50547.08	1.02 ± 0.30	3.50	0.11
50548.08	2.58 ± 0.37	3.56	
50549.07	1.94 ± 0.35	3.61	
50550.16	2.59 ± 0.64	1.20	0.12
50551.07	7.18 ± 0.68	2.53	0.12
50552.07	4.18 ± 0.44	3.65	0.11
50553.09	3.19 ± 0.67	1.58	
50555.15	3.83 ± 0.59	1.66	
50558.13	2.70 ± 0.60	2.27	
50559.14	5.50 ± 1.26	0.97	
50563.04	0.96 ± 0.46	4.10	0.13
50564.04	2.61 ± 0.52	4.01	
50565.05	1.65 ± 0.38	3.99	0.13
50566.05	1.41 ± 0.39	3.57	0.15
50567.09	1.13 ± 0.35	2.99	0.12
50568.07	0.78 ± 0.23	4.30	0.13
50569.07	1.10 ± 0.22	4.29	
50570.06	0.86 ± 0.19	4.23	0.13
50571.04	1.35 ± 0.20	4.37	0.11
50572.02	2.96 ± 0.26	4.53	0.12
50573.02	1.08 ± 0.19	4.18	0.13
50574.02	1.60 ± 0.20	4.69	
50575.01	3.11 ± 0.26	4.78	0.10
50576.02	4.55 ± 0.33	4.27	0.13
50577.02	4.30 ± 0.32	4.35	0.11
50578.00	2.95 ± 0.25	4.93	0.13
50579.00	3.43 ± 0.28	4.53	0.13
50580.01	2.98 ± 0.26	4.53	
50582.07	0.89 ± 0.35	1.19	
50583.04	4.42 ± 0.34	4.86	0.13
50584.08	2.47 ± 0.42	2.27	
50592.05	1.17 ± 0.51	3.46	0.12
50593.05	1.11 ± 0.47	3.49	
50597.97	0.62 ± 0.48	0.49	
50600.05	1.11 ± 0.47	0.50	
50601.06	1.59 ± 0.28	2.50	0.11
50603.05	3.20 ± 0.34	2.99	
50604.07	3.91 ± 0.42	2.41	0.16
50605.04	3.07 ± 0.35	3.00	0.12
50607.07	3.87 ± 0.48	1.92	0.11
50610.05	1.28 ± 0.28	2.41	0.12
50611.02	1.16 ± 0.26	1.99	
50612.04	2.61 ± 0.29	3.44	
50613.09	6.10 ± 0.60	1.89	
50615.98	0.78 ± 0.70	3.97	0.12
50616.96	0.43 ± 0.38	4.32	0.12
50622.95	4.93 ± 0.47	3.82	
50623.99	1.39 ± 0.45	2.31	0.11
50624.98	1.99 ± 0.32	2.99	0.11
50625.98	8.96 ± 0.62	2.49	0.10
50626.98	7.61 ± 0.47	3.46	
50628.07	5.23 ± 1.18	0.50	0.11
50628.96	1.25 ± 0.29	2.00	0.11
50629.95	0.54 ± 0.23	1.84	
50632.95	0.68 ± 0.23	2.00	0.14
50633.95	0.57 ± 0.19	3.00	0.12
50634.95	1.58 ± 0.26	3.00	0.12
50635.95	0.18 ± 0.19	2.50	
50636.93	0.27 ± 0.17	3.33	0.11
50637.98	0.86 ± 0.24	2.32	0.20
50638.95	4.67 ± 0.37	3.68	0.19
50639.98	3.71 ± 0.36	3.44	0.12
50640.98	3.66 ± 0.43	3.04	0.16
50641.95	3.10 ± 0.47	2.76	0.11
50642.94	6.38 ± 0.64	2.80	0.14
50643.91	2.52 ± 0.50	3.05	0.13
50650.94	1.98 ± 0.51	3.55	0.12
50651.94	1.76 ± 0.33	3.24	0.12
50653.93	2.31 ± 0.50	1.00	
50654.94	1.39 ± 0.40	1.30	
50657.92	1.62 ± 0.31	2.45	0.14
50658.90	0.62 ± 0.22	2.80	0.12
50659.90	0.94 ± 0.25	2.79	0.11
50660.90	1.33 ± 0.27	2.76	0.12
50661.90	1.54 ± 0.29	2.76	
50662.90	2.36 ± 0.34	2.67	
50663.90	4.98 ± 0.47	2.60	
50664.90	1.39 ± 0.28	2.49	0.16
50665.89	1.69 ± 0.32	2.00	0.18
50666.91	1.84 ± 0.46	1.00	0.11
50667.91	5.17 ± 0.73	1.33	
50668.89	1.57 ± 0.52	1.49	0.11
50669.90	3.30 ± 0.73	1.50	0.11
50670.89	0.35 ± 0.45	1.50	0.11
50671.89	1.50 ± 0.54	2.24	
50672.89	0.39 ± 0.53	2.19	0.11
50681.89	2.54 ± 0.57	1.00	0.10
50682.87	6.11 ± 0.82	1.49	0.10
50683.88	6.85 ± 0.71	1.50	
50684.87	1.89 ± 0.40	2.12	
50685.88	0.26 ± 0.27	1.98	
50686.88	0.79 ± 0.35	1.33	
50687.88	1.97 ± 0.41	1.95	0.10

Table 4. (continued)

Start [MJD]	Φ (E > 1.5 TeV) [10^{-11}cm^{-2}s^{-1}]	Duration [h]	Extinction [JohnsonV]
50688.88	0.32 ± 0.26	1.87	0.10
50689.87	0.49 ± 0.43	0.82	0.09
50691.88	2.13 ± 0.45	1.65	0.08
50692.89	1.03 ± 0.47	1.00	
50693.87	0.75 ± 0.37	1.16	0.12
50694.88	2.48 ± 0.50	1.49	
50695.87	3.58 ± 0.60	1.43	0.12
50696.87	0.17 ± 0.29	1.42	0.14
50697.86	0.19 ± 0.35	1.35	0.25
50700.87	1.52 ± 0.88	1.01	
50701.85	3.10 ± 0.96	1.23	
50702.88	-1.75 ± 0.46	0.46	
50703.85	0.83 ± 1.19	1.13	
50705.86	4.63 ± 2.20	0.73	
50706.84	1.47 ± 1.62	0.66	
50708.86	1.02 ± 1.21	0.79	
50709.85	0.26 ± 0.47	0.98	
50712.85	1.50 ± 0.74	0.69	
50713.84	0.98 ± 0.57	0.78	
50716.86	0.24 ± 1.72	0.12	
50717.85	-0.59 ± 0.48	0.33	
50719.84	2.34 ± 1.00	0.48	
50720.85	5.57 ± 2.59	0.13	
50721.83	0.33 ± 0.70	0.33	

3. The deferred analysis of the data taken at large zenith angles will add about 15% more data points on the light curve as well as reducing some of the errors of the shown data points.
4. The data point at MJD 50526 is less reliable because observations were carried out during strong and gusty winds.
5. The visibility at MJD 50697 was at the allowed limit, therefore this flux value may have to be corrected.
6. A detailed time structure analysis including also the data from large zenith angle observations (including observations under moonlight) is in preparation and will be published elsewhere.
7. No CT1/2 entries are shown after MJD 50721 because of modest statistics below 38° zenith angle.

6. Discussion and summary

The long period of intense flaring of Mkn 501 provided the unusual opportunity

a) to obtain a large and relatively clean sample of VHE γ-rays,
b) to carry out a detailed analysis of the spectral distribution and the lightcurve over a duration of nearly seven months,
c) to carry out multi-wavelength observations,
d) to compare the highly variable γ emission with that observed in previous years and also with that of other AGNs,
e) to test the detector performance by comparing data taken at the same time with nearby telescopes and in other experiments.

Table 5. Diurnal flux values above 1.5 TeV as measured by CT2. For some nights we list the Johnson V extinction coefficients (from the Carlsberg Automatic Meridian Circle).

Start [MJD]	Φ (E > 1.5 TeV) [10^{-11}cm^{-2}s^{-1}]	Duration [h]	Extinction [JohnsonV]
50523.14	1.74 ± 0.38	2.43	
50524.20	2.49 ± 0.49	1.17	
50540.10	2.14 ± 0.98	0.65	0.13
50545.18	1.95 ± 0.47	1.24	
50546.08	0.78 ± 0.29	3.34	0.10
50547.07	1.28 ± 0.32	3.50	0.11
50548.07	2.60 ± 0.35	3.54	
50549.07	2.63 ± 0.34	3.63	
50550.10	2.15 ± 0.33	2.69	0.12
50551.07	7.08 ± 0.57	2.47	0.12
50552.06	4.85 ± 0.40	3.49	0.11
50574.04	1.97 ± 0.47	1.50	
50575.05	3.32 ± 0.66	1.00	0.10
50577.05	5.60 ± 0.74	1.00	0.11
50578.02	4.91 ± 0.58	1.50	0.13
50599.97	1.17 ± 0.42	1.50	
50600.97	1.57 ± 0.38	1.96	0.11
50601.98	2.46 ± 0.40	2.00	
50604.95	4.22 ± 0.48	1.99	0.12
50606.97	5.36 ± 0.51	1.96	0.11
50607.96	2.95 ± 0.60	1.00	
50622.91	5.79 ± 0.84	0.83	
50623.90	3.71 ± 0.49	1.67	0.11
50624.91	2.55 ± 0.37	2.33	0.11
50625.92	7.54 ± 0.53	2.26	0.10
50626.91	8.37 ± 0.48	3.00	
50627.95	7.63 ± 0.50	2.80	0.11
50628.91	1.29 ± 0.29	2.83	0.11
50629.91	1.43 ± 0.49	1.00	
50630.90	0.11 ± 0.44	0.99	
50631.91	0.71 ± 0.44	1.00	0.11
50632.91	0.39 ± 0.44	0.99	0.14
50633.91	0.49 ± 0.44	1.00	0.12
50634.93	1.81 ± 0.75	0.50	0.12
50635.90	0.47 ± 0.44	0.95	
50636.91	0.36 ± 0.37	1.00	0.11
50637.94	0.67 ± 0.38	1.00	0.20
50638.96	4.21 ± 0.87	0.50	0.19
50653.91	2.39 ± 0.59	0.81	
50654.91	1.23 ± 0.65	0.49	
50657.90	1.73 ± 0.66	0.50	0.14
50658.90	2.51 ± 0.64	0.50	0.12
50659.90	1.50 ± 0.61	0.50	0.11
50660.90	1.94 ± 0.64	0.50	0.12
50661.90	2.04 ± 0.68	0.50	
50684.88	1.98 ± 0.44	1.76	
50685.88	1.61 ± 0.46	1.50	
50687.88	1.47 ± 0.55	1.00	0.10
50688.88	-0.05 ± 0.40	1.49	0.10

Most of the conclusions have already been presented in Part I. Here we concentrate on a comparison of data taken with the different HEGRA CTs and results related mainly to increased

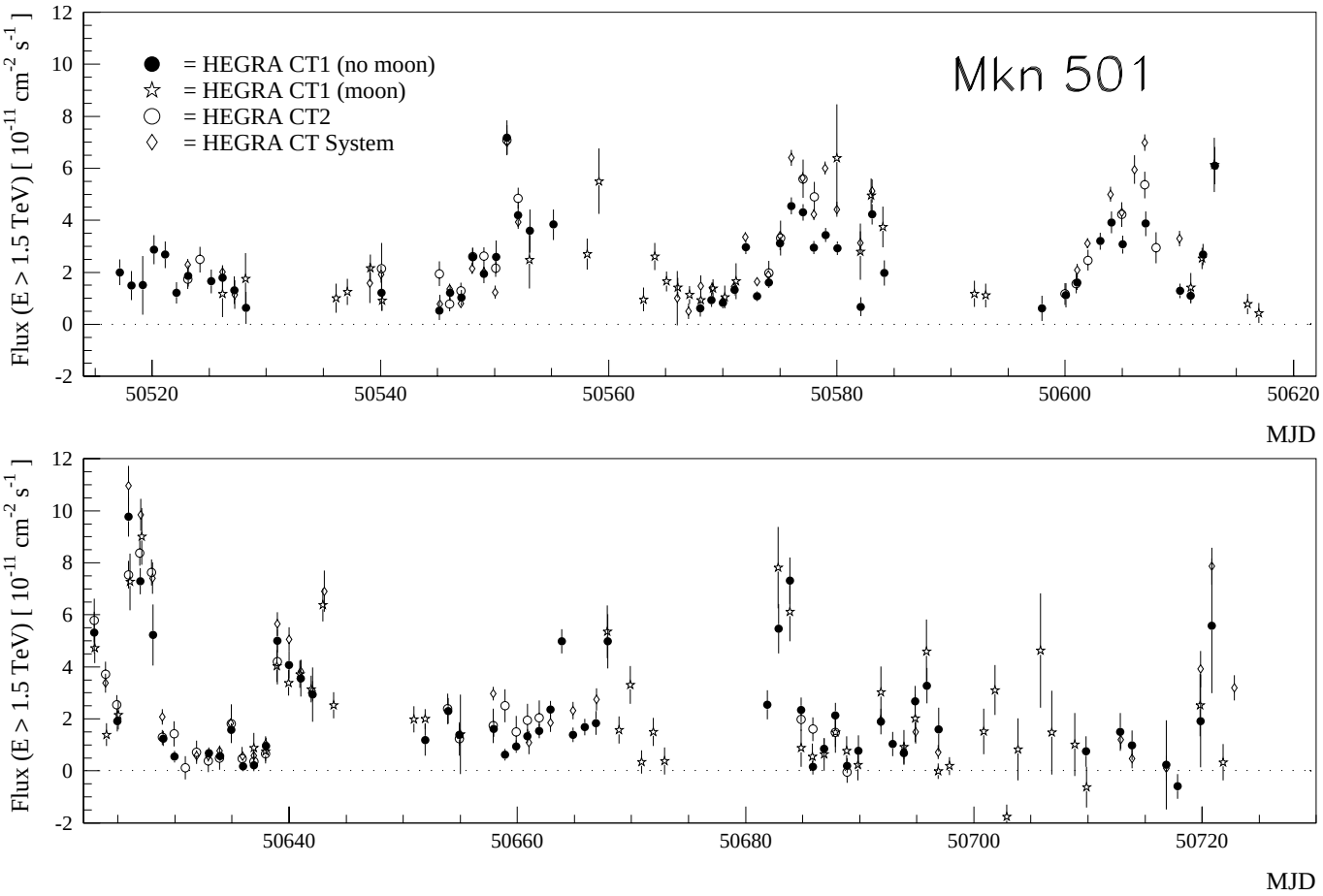

Fig. 14. The measurements of CT1 at all HV settings, with and without the presence of moonlight, and of CT2. All points are scaled to the threshold of 1.5 TeV using the spectrum measured in Sect. 3.1 and 4.1. The measurements of the CT system (Part I) are added for comparison.

density of nightly samplings and outline some future analysis prospects which will require additional measurements.

The data of CT1 and 2 presented here are for about half the time overlapping with the CT system observation periods, while the other half fills many gaps, dominantly during moonlit nights, but normally CT1 was also observing 30%-50% longer during dark nights. Nevertheless, even during identical times and given the fact that CT1 is basically centered to the system, not only identical events have been recorded. This is due to the collection area of the CT system being about 2 1/2 times larger than that of CT1. Also, due to the larger cameras and better precision on the impact parameter calculation, one could record with the CT system showers where one "sees" only shower halo particles, i.e., from showers with an impact distance between 130–200 m. Due to the different readout concept, 8 bit FADC readout of the CT system and 10 respectively 11 bit charge sensitive gated ADCs of the stand-alone telescopes, the saturation effects for multi-TeV showers are different. Also it should be mentioned that we used different MC programs for the standalone CT1/CT2 and the system. In addition we used quite different procedures for the γ selection. In spite of these differences we see in general excellent agreement in the structure of the lightcurve of the data recorded with the different instruments. In general, we see a better agreement between CT1 and CT2 data although their direct event overlap is smaller than that between the CT system and CT1 observations. The flux values from CT1 are systematically lower compared to the CT system data by about 27%. For the time being we are unable to decide whether this is related to the very different analysis methods or due to the systematic errors in the photon to ADC signal conversion ratio.

We observe good agreement of the spectral shape from the observations with the different telescopes. Fig. 15 shows a comparative plot where we combined the two resp. three zenith angle ranges of CT1 and CT2. Obviously, an unbroken power law will not describe the data well, except for the limited energy range of the CT1 data (see Sect. 3.1). An ansatz with an exponential cutoff

$$\mathrm{d}F/\mathrm{d}E \propto E^{-\alpha} \cdot e^{-E/E_0}$$

yielded:

for CT1: $\alpha = 2.09 \pm 0.09,\ E_0 = (7.16 \pm 1.04)$ TeV
with a reduced $\chi^2 = 0.6$ (fit to the data points of Fig. 5)

for CT2: $\alpha = 1.27 \pm 0.37,\ E_0 = (2.85 \pm 0.58)$ TeV
with a reduced $\chi^2 = 1.7$ (fit to the data points of Fig. 12)

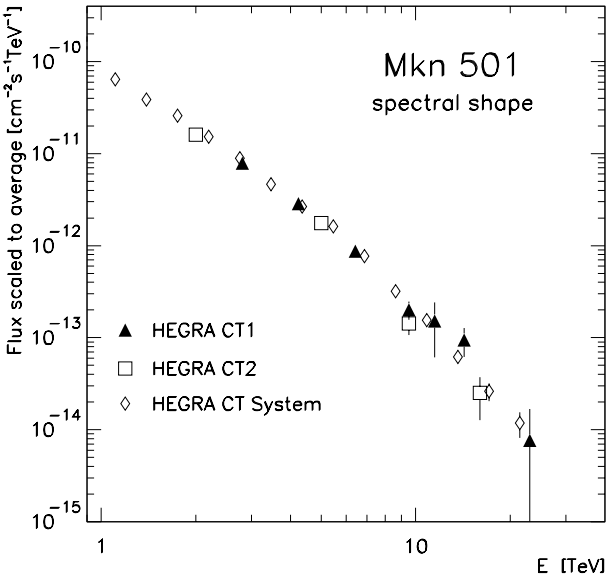

Fig. 15. The average spectral shape as measured by CT1, CT2 and the CT system (normalized at 4 TeV).

The fit to the preliminary data of the HEGRA IACT system in the energy region from 1.25 TeV to 24 TeV (Krawczynski 1998) gives:

for CT system: $\alpha = 1.9 \pm 0.05,\ E_0 = (5.7 \pm 1.1)$ TeV

It should be noted that α and E_0 are highly correlated, i.e., a modestly more curved spectrum enforces both a lower α and lower E_0 in the fit. This is particularly obvious for the CT2 data. The difference in the three sets of α and E_0 is explaineable by the different range of the fit. If we fit the CT2 spectrum using the 'system' α of 1.9 we obtain an $E_0 = (5.3 \pm 0.4)$ and a slightly worse reduced χ^2 of 1.9.

The observed steepening of the spectrum could be either due to an inherent change in the acceleration and interaction process or due to γ-interaction with the cosmic IR background. A detailed study of the spectra will be presented in a forthcoming paper.

Other tests of the existence of an IR absorption have been proposed by Aharonian et al. (1994) and Plaga (1995), namely the production of pair halos and time delay of secondary γs. The "halo" γs should show up predominantly at larger ALPHA values and should not show the rapid variation of the main γ flux at all. Another aspect is that, depending on the onset of the IR absorption, the spectrum of the halo γs should be much softer resp. have a lower energy cutoff. The effect should be quite visible in the 1–10 TeV region if strong IR absorption occurs above 25–35 TeV. We searched for such effects using data between 10° to 20° in ALPHA but no conclusive results could be drawn due to insufficient statistics. One of the problems is that improvements in the source position resolution due to higher energy can fake a soft halo spectrum. Also the wide spread of the prediction for the extragalactic magnetic field make such an analysis difficult.

Due to the large number of CT1 daily flux measurements a precise comparison with the nearly continuous RXTE data is possible. The correlation of 0.61 ± 0.06 between the CT1/2 data and the RXTE data gives a rather strong evidence of a coupled effect such as electron acceleration and inverse Compton scattering on synchroton radiation generated photons.

Close inspection of the data show that around MJD 50580 the structure of the lightcurve in the TeV range differs significantly from that at the 2–10 keV range. While observing significant flaring in the TeV range, the keV lightcurve remaines constant within errors. If we exclude the data between MJD 50568 and 50590 the correlation rises to 0.65 ± 0.07 while inside the range it drops to 0.17 ± 0.19.

The assumption of the electron acceleration gets further support from the about quadratic rise of TeV γ flux as compared to the keV flux rise from 1996 to 1997, see Sect. 3.5. Clearly, a long term observation of the keV – TeV correlation over a few years should give further support or disprove the concept of electron acceleration dominance. Hadronic components and/or a significant change in electron acceleration cannot be ruled out, see our comment on the observation around MJD 50580.

Note that the 1996 Mkn 501 data, originally showing a 5.8 σ excess (Bradbury et al. 1997), have been reanalysed using the dynamical supercuts also used in this paper. The excess increased to $> 7\sigma$ while the flux values and the integral spectrum remained the same ($F(E > 1.5\mathrm{TeV}) = 2.3 \times 10^{-12}\mathrm{cm}^{-2}\mathrm{s}^{-1}$). Comparing the 1996 and the 1997 spectrum, however, we find indications that the curvature of the spectrum has increased since the increase in flux from 1996 to 1997 is lower at higher energies. A detailed comparison between the spectra in 1996 and 1997 will be presented in a later paper.

Finally, we want to comment on a technical conclusion drawn from the analysis. For precision measurements it is important to use a larger camera diameter compared to the one of CT1. A larger camera would have resulted in a significantly better energy and angular resolution at higher energies.

Acknowledgements. The HEGRA collaboration thanks the Instituto de Astrofisica de Canarias and the town of Garafia for use of the site and the excellent working conditions. Also we acknowledge the rapid availability of the RXTE data and the atmospheric extinction data from the CAMC. This work was supported by the German Ministry of Education and Research, BMBF, the Deutsche Forschungsgemeinschaft, DFG, and the Spanish Research Foundation CICYT.

References

Aharonian F.A., Coppi P.S., Voelk H.J., 1994 ApJ 423, L5
Aharonian F.A., Akhperjanian A.G., Barrio J.A., et al., 1999, A&A 342, 69A, see also astro-ph/9808296
Blobel V., 1984, Unfolding Methods in high-energy physics experiments. DESY 84–118, Hamburg
Blobel V., 1996, OPAL Technical Note TN361, CERN, Geneva
Bradbury S.M., Deckers T., Petry D., et al., 1997, A&A 320, L5
Carter-Lewis D.A., Biller S., Boyle P.J., et al., 1997, In: Proc. 25th ICRC, Durban, 3, 161
Konopelko A., Aharonian F.A., Akhperjanian A.G., et al., 1996, Astropart. Phys. 4, 199
Kranich D., 1997, Diploma Thesis, MPI-PhE/97–11
Kranich D., Deckers T., Lorenz E., et al., 1997, In: Proc. 4th Compton Symposium, Williamsburgh, 2, 1407

Kranich D., Mirzoyan R., Petry D., et al., 1998, Astropart. Phys. submitted
Krawczynski H., 1998, In: Proc. BL Lac Phenomenon Meeting, Turku, in print
Lindner A., 1997, In: Proc. 25th Cosmic Ray Conference, Durban, 5, 113
Marquardt P.R., 1963, Journal of the Society for Industrial and Applied Mathematics 11, 431
Mirzoyan R., Kankanian R., Krennrich F., et al., 1994, NIM A 351, 513
Plaga R., 1995, Nat 374, 430
Petry D., Bradbury S.M., Konopelko A., et al., 1996, A&A 311, L13
Petry D., 1997, Ph.D. Thesis, Max-Planck-Institute for Physics, Munich, report MPI-PhE/97–27
Petry D., Kranich D., 1997, In: de Jager O.C.(ed.) Towards a major atmospheric Cherenkov detector V, Kruger Park, 368
Protheroe R.J., Bhat C.L., Fleury P., et al., 1997, In: Potgieter M.S., et al. (eds.) Invited, Rapporteur and Highlight Papers at the 25th International Cosmic Ray Conference, 317
Quinn J., Akerlof C.W., Biller S., et al., 1996, ApJ 456, L83
Rauterberg G., Müller N., Deckers T., et al., 1995, In: Proc. 24th International Cosmic Ray Conference, Rome, 3, 460
Tanimori T., Sakurazawa K., Dazeley S.A., et al., 1998, ApJ 492, L33
Wiedner C.A., 1994, In: Kifune T. (ed.) Towards a major atmospheric Cherenkov detector III, Tokyo, 119